Journal of Volcanology and Geothermal Research 381 (2019) 273–283

Contents lists available at ScienceDirect

Journal of Volcanology and Geothermal Research

journal homepage: www.elsevier.com/locate/jvolgeores

Three-dimensional kernel-based coda attenuation imaging of caldera structures controlling the 1982-84 Campi Flegrei unrest

Waheed Gbenga Akande [a,b,*], Luca De Siena [a,c], Quan Gan [a]

[a] University of Aberdeen, School of Geosciences, Geology and Petroleum Geology Department, Meston Building, King's College, Aberdeen AB24 3UE, Scotland, UK
[b] Federal University of Technology, School of Physical Sciences, Geology Department, Bosso Campus, PMB 65, Minna, Nigeria
[c] Institute of Earth Sciences, Johannes Gutenberg University Mainz, Mainz, Germany

ARTICLE INFO

Article history:
Received 3 February 2019
Received in revised form 11 June 2019
Accepted 12 June 2019
Available online 14 June 2019

Keywords:
Campi Flegrei
Coda waves
Geothermal
Seismic attenuation
Seismic tomography
Unrest

ABSTRACT

Coda-wave attenuation imaging has risen as a state-of-the-art technique to depict volcanic structures using their dispersion effects. The 1982–84 seismic and deformation unrest at Campi Flegrei caldera (Italy) is a unique example of non-eruptive volcanic activity in a structured caldera. Here, we propose the first application of 3D coda-attenuation kernels to image caldera structures at multiple frequencies during unrest. Using sensitivity kernels is necessary to assess the effective resolution of coda imaging in highly heterogeneous volcanoes. The technique relies on the solution of Paasschens' equations in the framework of radiative transfer theory. The results map coda attenuation in the 3D space without need of pre-existent velocity models. The resolution and stability of the inversion solutions were examined by changing the damping parameters and outputting the corresponding images, inverting for different node spacings and performing checkerboard tests. These tests show that the resolution of the multiple-scattering model is much lower than that provided by a standard isotropic-scattering and/or single scattering technique. The best resolution in our model is obtained between depths of 1 km and 3 km in the centre of the model, between Pozzuoli town and Solfatara crater. The results are discussed at a frequency of 3 Hz, due to both longer coda durations and broader kernel illumination: in this frequency range, coda-based 3D imaging had so far failed to provide stable results. The interpretation is performed based on the extensive geological and geophysical knowledge of the caldera. High-attenuation anomalies below Solfatara and Monte Nuovo mark areas either saturated with water or enriched in molten rocks, feeding the respective fumarole fields. The flattening and horizontal elongation of these anomalies below 2 km depth is a manifestation of the blocking and spreading around of the rising hot magmatic fluids below a previously-inferred high-velocity, low-attenuation and highly-deforming caprock. This caprock is not uniform, likely due to the remnants of erupted structure. A SW-to-NE-trending low-attenuation and high-velocity anomaly deeps down to 3 km under Pozzuoli. We infer that the high seismicity in the region is a consequence of the stress sustained by the caprock from a 4-km-deep deformation source in 1983–84. On top of this source, high coda attenuation corresponds to high Vp/Vs ratios and high direct-wave attenuation. The region's characteristics are likely due to the accumulation of magmatic fluids above a magmatic sill.

1. Introduction

Coda waves are incoherent, complex and late-arriving seismic signals recorded in high-frequency seismograms produced by earthquakes or active seismic experiments. They are generated from the complex interaction of seismic waves with the heterogeneous medium between source and station (Sato et al., 2012). A successful interpretation of the physical mechanisms causing coda waves (and their attenuation) requires the understanding of the effect of seismic attenuation and its two main constituents, scattering and absorption (Aki and Chouet, 1975). Total seismic attenuation is described by a quality factor (Q), which is the ratio between the total energy and the energy lost in one cycle. The inverse quality factor (Q^{-1}) is a measure of the energy lost into the medium by seismic waves while they propagate. The direct P- and S-waves Q^{-1} (i.e., Q_p^{-1} and Q_s^{-1}) measure the seismic wave amplitude losses of coherent wave-packets propagating as a ray between the source and receiver. Attenuation tomography traditionally maps these coherent parameters. Coda wave attenuation (Q_C^{-1}) measures instead the decay of the wave intensity with increasing lapse time from the origin time of the earthquake (Fig. 1). As Q^{-1}, Q_C^{-1} is a complex mixture of the inelastic and the heterogeneous properties of the medium.

* Corresponding author at: University of Aberdeen, School of Geosciences, Geology and Petroleum Geology Department, Meston Building, King's College, Aberdeen AB24 3UE, Scotland, UK.
E-mail address: waheed.akande@abdn.ac.uk (W.G. Akande).

https://doi.org/10.1016/j.jvolgeores.2019.06.007
0377-0273/

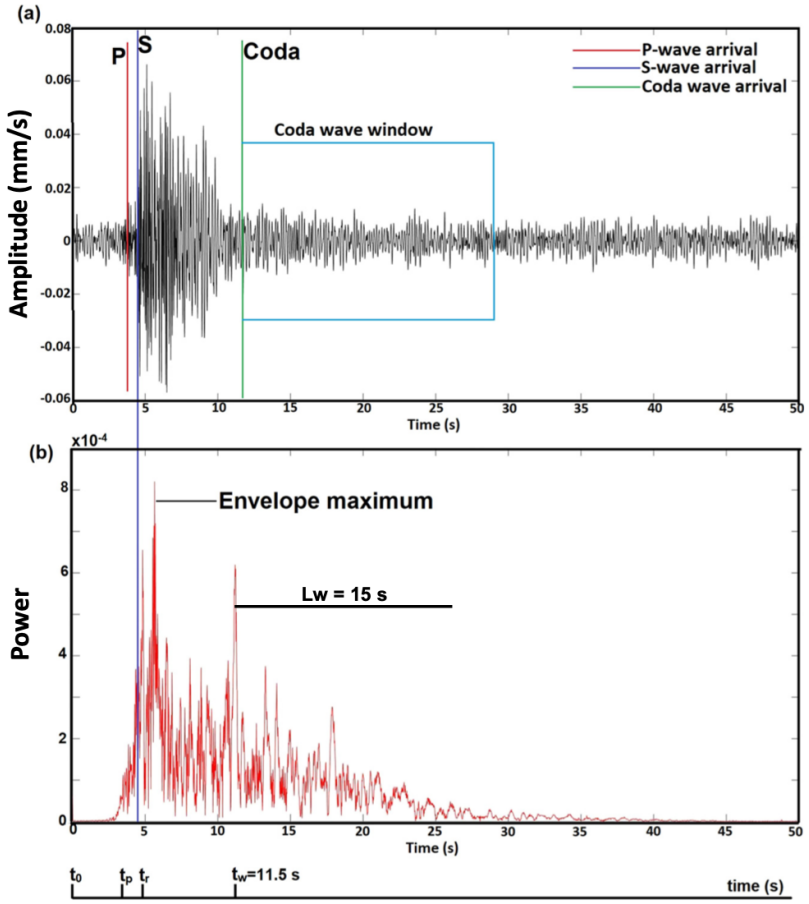

Fig. 1. A sample raw seismogram and calculated envelope. Panel (a) shows P- and S-arrivals as well as the time-window where coda-wave energies are higher than twice the noise at all frequencies (3, 6, 12 and 18 Hz). Panel (b) shows time-widow used to compute the coda-energy; t_0, t_p, t_r, t_w and Lw are the origin time, P-wave arrival time, S-wave arrival time, starting time for the window and length of the window used for modelling the smoothed envelope, respectively.

Inelastic properties induce friction that converts elastic energy into heat, causing intrinsic attenuation, Q_i^{-1}. The interaction of an incident seismic wave with heterogeneities redistributes this energy into the coda, inducing scattering attenuation, Q_{sc}^{-1} (Padhy and Subhadra, 2013). The physical interpretation of Q_C^{-1} is thus controversial due to possible co-existence of coherent and stochastic wavefields in the pre-defined coda window (Fig. 1).

Researchers can obtain average estimates of intrinsic and scattering attenuation from coda waves, e.g., via the Multiple Lapse Time Window Analysis (MLTWA - Bianco et al., 2002; Mukhopadhyay et al., 2010; Del Pezzo et al., 2011; Padhy and Subhadra, 2013). These estimates, which discriminate between mechanisms inducing coda, are available at Campi Flegrei caldera (Del Pezzo et al., 1995). They additionally provide measures of background Earth's heterogeneity, which allows us to model sensitivity of seismogram envelopes theoretically and computationally in space (e.g., Calvet and Margerin, 2013; Calvet et al., 2013; De Siena et al., 2013; Margerin et al., 2015; Del Pezzo et al., 2016; Del Pezzo et al., 2018). The reconstruction of coda envelopes in space has led to the recent development of coda-wave attenuation tomography, providing images of scattering, absorption, and coda attenuation in space at lithospheric scale (Vargas and Mann, 2013; Calvet et al., 2013; Mayor et al., 2016; Borleanu et al., 2017).

Seismic attenuation imaging is useful in delineating structures such as fractures, fluid-saturated rocks, thermal (or hot) zones including melts or magma, and hydrothermal or magmatic fluids (e.g., Winkler and Nur, 1979; Spencer, 1981; De Siena et al., 2010). 2D coda-attenuation imaging is thus today widely applied to map attenuation in volcanic and geothermal areas (e.g., Prudencio et al., 2013a, 2013b, 2018). Together with 3D direct P- and S-wave attenuation tomography, 2D coda-wave attenuation mapping has been successful at recovering fluid, magmatic, and fault structures in active volcanic settings across four continents:

1. Europe – Mt. Vesuvius (Del Pezzo et al., 2006; De Siena et al., 2009, 2017a), Stromboli (Prudencio et al., 2015c), Campi Flegrei caldera (De Lorenzo et al., 2001; De Siena et al., 2010; De Siena et al., 2017a, 2017b), and Tenerife Island (Prudencio et al., 2015b);
2. America – Mount St. Helens (De Siena et al., 2014a), Galeras (Vargas et al., 2012);
3. Asia – Asama (Prudencio et al., 2017a) and Usu (Prudencio et al., 2017b) volcanoes;
4. Antarctica – Deception Island (Prudencio et al., 2015a).

Campi Flegrei is the volcano where the highest number of attenuation imaging techniques using both direct and coda wavefields have been applied. The first attenuation study (De Lorenzo et al., 2001) used pulse-width data to invert for the 3D P-wave attenuation structure of the caldera. It was followed by the 3D single-scattering tomography of Tramelli et al. (2006), producing a model of single scattering coefficient variations across the caldera. De Siena et al. (2010) used the standard t^* (or spectral slope) method and a new coda-normalization method to model both P- and S-wave attenuation across the caldera:

the coda-normalization process tries to reduce the biases induced by the source and station contributions on attenuation observations by assuming that coda observations are constant in space (limited *Qc* variations). This assumption was based on the small variations in scattering coefficients obtained by Tramelli et al. (2006) inside the caldera. De Siena et al. (2017b) apply again the coda-normalization method, this time removing the assumption of constant coda attenuation throughout the medium. A novel take on coda-wave imaging in volcanoes is to compute coda-wave sensitivity kernels (e.g., Del Pezzo et al., 2016) and target areas affected by high deformation. De Siena et al. (2017a) map the coda attenuation variations in 2D using an analytic approximation of radiative-transfer-derived kernels (Del Pezzo et al., 2016). Calò and Tramelli (2018) apply the t^* (total attenuation) and single-scattering tomography methods using an advanced tomographic framework originally developed for velocity tomography.

The 2D coda-wave attenuation mapping based on approximate kernels (De Siena et al., 2017a) resolved two high-attenuation areas at a frequency of 3 Hz in the caldera, the most difficult to model due to anomalous scattering effects induced by the shallow fractured medium (De Siena et al., 2013). The first anomaly was interpreted as fluid-bearing reservoirs that are connected with the subsidence regime acting near Mount Nuovo after the 1983–84 caldera unrest (Capuano et al., 2013). The second anomaly maps local fumarole feeders in the restless NE onshore part of the caldera. In De Siena et al. (2017a), a single low coda-attenuation anomaly that coincides with the area of maximum deformation (Amoruso et al., 2014) and lowest density (Amoruso et al., 2008) was resolved during the 1983–84 unrest. The authors interpreted it as an evidence of the bending in the "caprock" derived by rock-physics experiments as a continuous boundary under Campi Flegrei (Vanorio and Kanitpanyacharoen, 2015), which blocks the propagation of the magmatic materials to the surface. A recent seismic tomography (Calò and Tramelli, 2018) locates a low-velocity and high-attenuation volume in the same area at depths of 2.2 to 3.5 km. A high Vp/Vs is interpretable as magmatic if it corresponds to high attenuation, especially with high absorption (De Siena et al., 2014b); however, 3D direct-wave attenuation imaging offers little resolution in this area and depth range due to the limitation of the ray-dependent technique (De Siena et al., 2017b; Calò and Tramelli, 2018).

De Siena et al. (2017a) highlighted the need for three-dimensional coda attenuation imaging at the Campi Flegrei caldera based on more exact computational kernels. 3D sensitivity kernels for coda attenuation have been developed theoretically and computationally and applied to test datasets at Deception Island and Mount St. Helens (Del Pezzo et al., 2018). These tests prove the applicability of 3D coda-attenuation imaging when targeting the first three-four kilometres of the crust. The kernels represent a significant advancement, as it allows overcoming the single-scattering approximation generally used in scattering tomography (Nishigami, 1991; Tramelli et al., 2006; De Siena et al., 2014a; Calò and Tramelli, 2018). The work we present here is the first tomography performed using multiple-scattering coda sensitivity kernels (Paasschens' approximation – Paasschens, 1997) to invert for 3D coda attenuation; with respect to the scattering tomography of Tramelli et al. (2006) and Calò and Tramelli (2018), it adds multiple scattering sensitivity kernels to the inversion, which are more appropriate to image the volcano. De Siena et al. (2017a) used only the approximative diffusive part of the kernels and applied it to a 2D inversion. The objective of this study is to obtain a 3D coda attenuation model of the 1983–1984 unrest for the caldera at 3 Hz. This model is expected to give further insights into the large-scale volcanic structures and fluid-flow dynamics triggering volcanic activity at the caldera.

2. Geological and geophysical settings, and volcanological history of the Campi Flegrei caldera

Campi Flegrei caldera (CFc, west of the city of Naples – Fig. 2) is in the Campanian Plain, between the eastern side of the Tyrrhenian Sea and the southern Apennines chain. Its geological history is connected with the regional extension tectonics that affected the entire Plain (Orsi et al., 1996; Aiello et al., 2014). The Pliocene-Quaternary extensional fracture systems, trending predominantly NW-SE and NE-SW (Orsi et al., 1996), have important implications for the seismotectonic evolution of the caldera. The caldera represents one of the Phlegrean

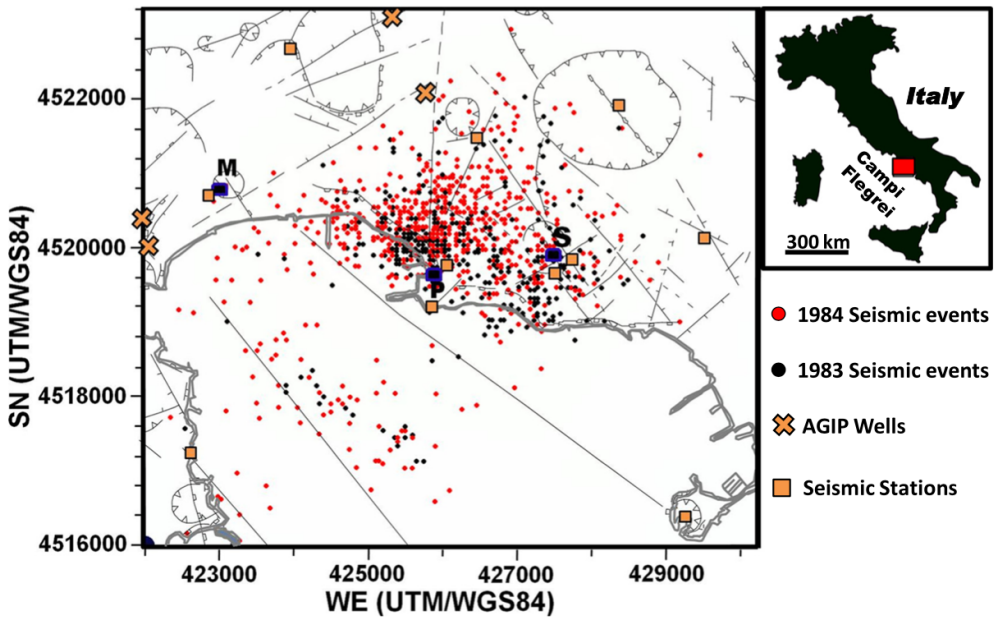

Fig. 2. Map of Campi Flegrei showing the seismicity of 1983–1984, fracture systems, the locations of seismic stations deployed by Wisconsin's University (four of which are outside the boundaries of the map) and AGIP wells. M, P and S are locations of Mount Nuovo, Pozzuoli and Solfatara, respectively. Thin black lines and curves represent the fracture systems at the caldera. Thick grey curves represent the coastline.

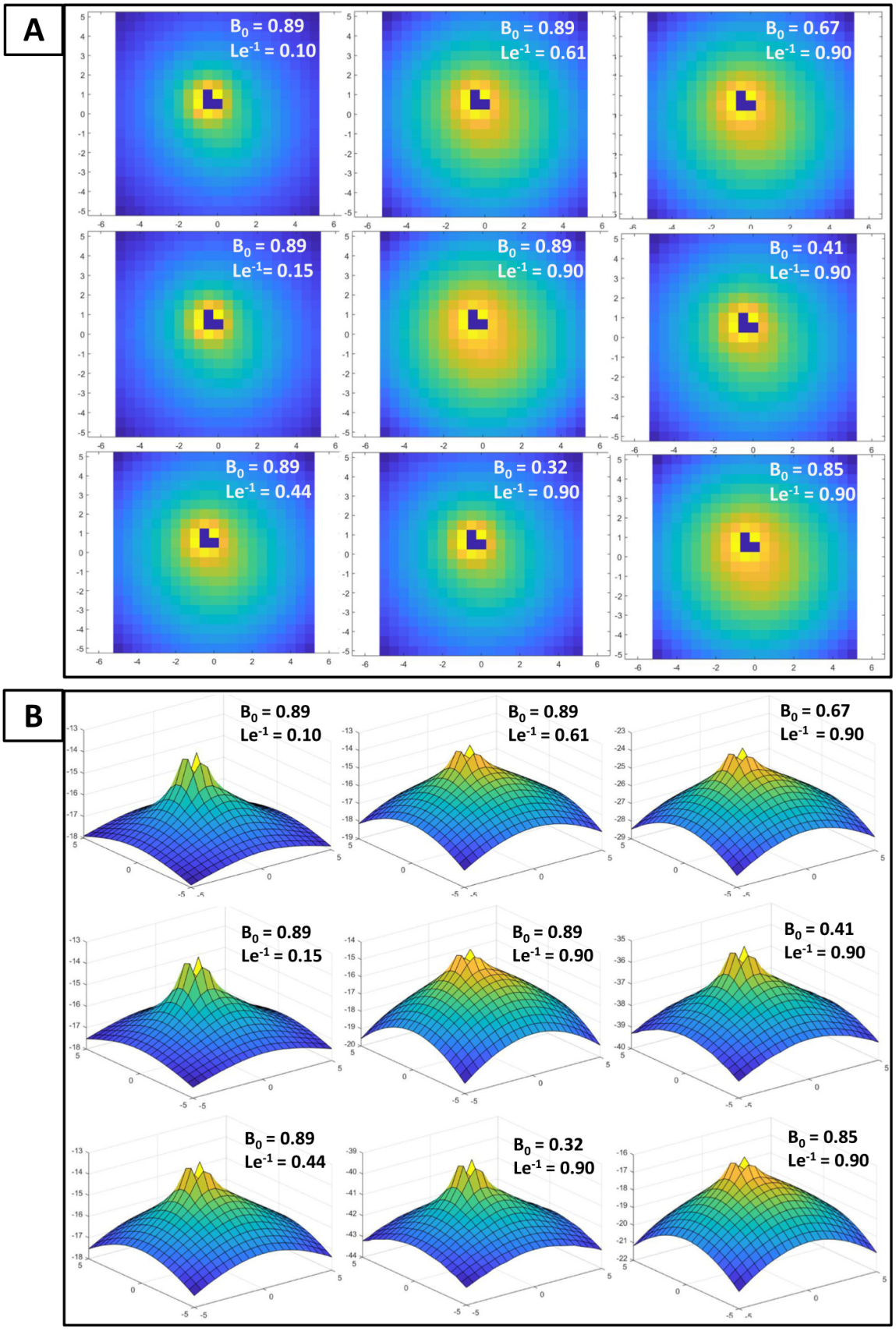
A
B_0 = 0.89
Le^{-1} = 0.10
B_0 = 0.89
Le^{-1} = 0.61
B_0 = 0.67
Le^{-1} = 0.90
B_0 = 0.89
Le^{-1}= 0.15
B_0 = 0.89
Le^{-1} = 0.90
B_0 = 0.41
Le^{-1}= 0.90
B_0 = 0.89
Le^{-1} = 0.44
B_0 = 0.32
Le^{-1} = 0.90
B_0 = 0.85
Le^{-1} = 0.90
B
B_0 = 0.89
Le^{-1} = 0.10
B_0 = 0.89
Le^{-1} = 0.61
B_0 = 0.67
Le^{-1} = 0.90
B_0 = 0.89
Le^{-1} = 0.15
B_0 = 0.89
Le^{-1} = 0.90
B_0 = 0.41
Le^{-1} = 0.90
B_0 = 0.89
Le^{-1} = 0.44
B_0 = 0.32
Le^{-1} = 0.90
B_0 = 0.85
Le^{-1} = 0.90

Fields' volcanic districts, where volcanism has been active for at least 50,000 years (Aiello et al., 2014). The modern-day geomorphic features in the volcanic district are results of volcano-tectonic events that occurred after the emplacement of the huge pyroclastic flow popularly referred to as the Campanian Ignimbrite (CI), erupting about 37,000 years ago, which represents when the area experienced the first episode of calderisation (Barberi et al., 1978; Orsi et al., 1996). The second phase of caldera formation is represented by the Neapolitan Yellow Tuff (NYT) eruption in about 12,000 years ago, making the CFc a twin-nested caldera (Orsi et al., 1996).

Orsi et al. (1991) have systematically described the geology of Campi Flegrei and its neighbourhood by using integrated data from surface outcrops and shallow drilled cores and logs. The surface and near-surface geology comprises pyroclastics, marine and palustrine sediments, and reworked deposits. The pyroclastic deposits are considered to be products of volcanic and phreatomagmatic, and phreatoplinian-phreatomagmatic eruptions of the CI and NYT caldera systems, sourced from magma ranging in compositions from trachyte to phonolitic-trachyte, and alkali-trachyte to latite, respectively (Orsi et al., 1991). This wide range of compositions has been corroborated by recent geochemical and mineralogical data reported by Carlino et al. (2018). The reports of the wells drilled by AGIP (1987) offered first-hand information on the subsurface geology, and from which the stratigraphy of the region has been reconstructed by Piochi et al. (2014) to reveal both vertical and lateral variations in the geology. In addition, Mesozoic carbonates have also been reported in the subsurface of CFc (Brocchini et al., 2001; Vanorio and Kanitpanyacharoen, 2015), and they have been hypothesized to play a significant role in strengthening the mechanical properties of the caprock in relation to microseismicity at Campi Flegrei (Vanorio and Kanitpanyacharoen, 2015).

At CFc, recent 3D S-wave attenuation mapping and 4D seismic studies (De Siena et al., 2017b) reveal a low-velocity (Vanorio et al., 2005) and high-attenuation hydrothermal reservoir between 3 and 4 km, active during the 1983–84 CFc unrest (1.8 metres ground uplift, and hundreds of earthquakes per day, but no eruption). The reservoir, still low-velocity during the last deformation unrest (De Siena et al., 2018) connects a 4–4.5 km deep aseismic high attenuation anomaly, either a magmatic sill or magmatic reservoir (De Siena et al., 2017b), to vents at the surface. The onset of wave-induced flow attenuation in reservoirs of multiphase magmatic fluids attenuates P- and S-waves in the presence of heterogeneous saturation. This mechanism could explain the high-attenuation anomalies mapped between 3 and 4.5 km depth at the caldera (De Siena et al., 2017b). All recent tomographic results (De Siena et al., 2017b; Calò and Tramelli, 2018) support the existence of a caprock possibly responsible for the lack of an eruption in 1982–84 (Vanorio and Kanitpanyacharoen, 2015). Calò and Tramelli (2018) model this caprock in 3D as overlying high Vp/Vs materials in the zone of maximum deformation, offshore Pozzuoli: this feature confirms the magmatic characteristics of the anomalies in the area.

3. Materials and method

3.1. 3D kernels modelling coda attenuation

The late-lapse-time 3D scattering regime at the CFc is diffusive at frequencies above 3 Hz a few seconds after the S-wave arrival (e.g., De Siena et al., 2013). Nevertheless, neither a single-scattering approximation nor diffusion can model caldera structures or seismic envelopes at 3 Hz (Tramelli et al., 2006; De Siena et al., 2013): this is due to the heterogeneous structure of the caldera, which enhances multiple-scattering effects across the entire envelope. Paasschens (1997) provides the solution to the equation of radiative transfer in three

Table 1
Frequency bandwidths of corner/central frequencies (f_c) of 3, 6, 12 and 18 Hz.

f_{low}	f_c	f_{high}
2	**3**	4
4	**6**	8
8	**12**	16
12	**18**	24

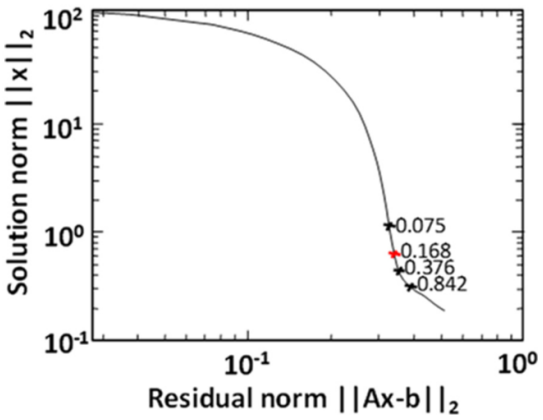

Fig. 4. L-curve with a chosen optimal damping parameter (red cross) for the linear inversion at 3 Hz. (For interpretation of the references to colour in this figure legend, the reader is referred to the web version of this article.)

dimensions, which includes both the diffusive and the multiple scattering regimes:

$$E^{3D}[r,t] \approx \frac{W_0\ \exp\left[-Le^{-1}vt\right]}{4\pi r^2 v}\ \delta[t-\frac{r_{ij}}{v}] + W_0 H[t-\frac{r_{ij}}{v}] * \frac{(1-\frac{r_{ij}^2}{v^2t^2})^{1/8}}{\left(\frac{4\pi vt}{3B_0Le^{-1}}\right)^{3/2}} * \exp\left[-Le^{-1}vt\right]\ F\left[vtB_0Le^{-1}\left(1-\frac{r_{ij}^2}{v^2t^2}\right)^{3/4}\right] \quad (1)$$

and

$$F\,|\,x\,| \approx e^x\sqrt{1+2.026/x} \quad (2)$$

where v is the wave speed in the half-space, r_{ij} is the distance of the source(i)-receiver(j) pair, x is the space coordinate along the direct wave propagation from the source, W_0 is the total incident wave energy at $t = 0$ and is assumed equal to 1, δ is the Dirac function, $H(x)$ is the Heaveside unit step function, t is the lapse-time from the origin, f is the frequency, r is the hypocentral distance, and B_0 and Le^{-1} are seismic albedo and inverse extinction length, respectively. The last two parameters are related to the attenuation coefficients by:

$$B_0 = \frac{\eta_{sc}}{\eta_{sc}+\eta_i} = \frac{Q_{sc}^{-1}}{Q_{sc}^{-1}+Q_i^{-1}}; Le^{-1} = \eta_{sc}+\eta_i = \frac{2\pi f}{v}\left(Q_{sc}^{-1}+Q_i^{-1}\right) \quad (3)$$

where η_{sc} and η_i are the scattering and intrinsic attenuation coefficients, and Q_{sc}^{-1} and Q_i^{-1} are scattering attenuation and intrinsic attenuation, respectively.

Del Pezzo et al. (2018) extended to 3D the 2D weighting functions (Del Pezzo et al., 2016) previously developed for volcanic media. In this work, Paasschens' equations are solved computationally; the

Fig. 3. (a) Map-view and (b) 45° angle view of the 3D Q_c sensitivity kernel obtained at a depth of 1 km for a single source-station pair. In the inversion the pole at the station location was interpolated using the nearest values. B_0 and Le^{-1} show the relative average contributions of scattering and intrinsic attenuation. The zero of the grid corresponds to the UTM (WGS84) coordinates [427000 4520000 0]. (For interpretation of the references to colour in this figure, the reader is referred to the web version of this article.)

solutions present poles at both source and station positions, common to most of the kernels today available in literature. Here, we built effective sensitivity kernels to invert Q_c in the 3D space: we account for the poles at source and station positions (Fig. 3, blue area at the centre of the yellow zone) by interpolation, using energy values modelled at nearby nodes. Del Pezzo et al. (2018) apply the kernels as space-weighting

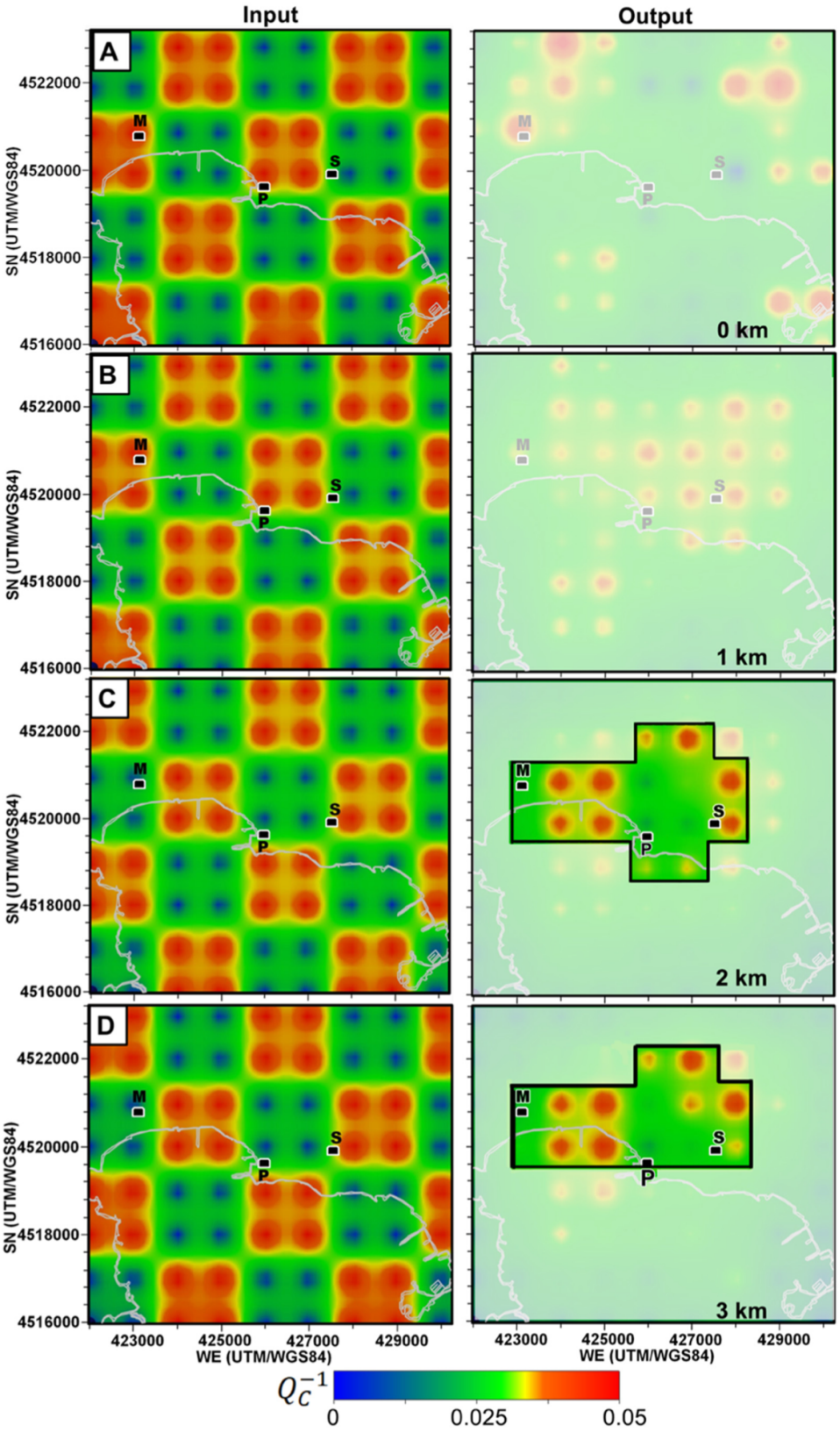

functions in regionalisation to model the active volcanic setting at Deception Island, Antarctica, in 3D and down to 4 km. Here, we propose the use of these kernels in an inversion for the 3D coda attenuation parameters at CFc, using the data of the 1984 seismic unrest. We thus precomputed the 3D sensitivity of each source-station Q_c measurement on a 3D grid with nodes spaced 0.5 km and 1 km, respectively, comprising the entire CFc (Fig. 3). We assume absorbing boundaries – hence all energy scatters inside the grid, which allows us to perform an inversion like that proposed by De Siena et al. (2017a) for the 2D case.

3.2. Application to the 1983–1984 seismic unrest dataset at CFc

The dataset used in this study consists of a subset of over 10,000 seismic events recorded in 1983–1984 seismic unrests by 20 permanent seismic stations of Osservatorio Vesuviano and Aquater AGIP and 15 temporary three-component stations deployed by the University of Wisconsin (Aster et al., 1989; Battaglia et al., 2008). The 20 permanent stations are single-(vertical)-component and provided the P- and S-wave pickings used to locate earthquakes throughout the unrest (De Siena et al., 2017a, 2017b). The P- and S-wave arrivals were also picked on the temporary stations, leading to a total of 7,264 P and 3,121 S arrival times available (Vanorio et al., 2005). The shear-wave 3D image of the attenuation structures was obtained using seismograms recorded between January 7, 1984 and April 14, 1984 by the 3-component temporary stations deployed by the University of Wisconsin (De Siena et al., 2017a, 2017b) – for a total of 2559 waveforms. Thus, the data (waveforms) used for the study are those from the Wisconsin's stations, which are portable three-component digital networks. This secondary dataset consists of 1,209 microearthquakes ($1.8 \le Md \le 4.0$)). The waveforms were modelled in a coda window starting at times much greater than twice the S-wave arrival, assuming a diffusive wavefield (see De Siena et al., 2013 for an estimation of the uncertainties of this assumption at Campi Flegrei). The novel 3D coda attenuation kernels described in Section 3.1 were applied to the dataset to model Q_C^{-1} in space.

We measured source-station Q_C^{-1} by fitting 15 s of the S-wave smoothed envelope after 11.5 s from the origin time with a decreasing exponential (Fig. 1b) and filtering in four frequency bands (Table 1). We use the standard exponential relationship between coda envelope decrease and Q_C^{-1} (Eqs. (4a) and (4b)) proposed by Aki and Chouet (1975) with a 3D multiple scattering time-decay factor of 1.5 (Paasschens, 1997; Calvet and Margerin, 2013):

$$E(t,f) = S(f)t^{-\alpha}e^{-2\pi ft/Q_c(f)} \tag{4a}$$

where $E(t, f)$ is the energy envelope, $S(f)$ is a frequency-dependent source and/or site term, t is the lapse time, f is the frequency, α is a positive exponent, and Q_c is the frequency-dependent quality factor of coda waves. We linearized the relationship by taking the logarithm:

$$\ln E(t,f) = \ln S(f) - \alpha \ln t - 2\pi ft/Q_c(f) \tag{4b}$$

and fitted the energy vs time data with a line. In the inversion, we only kept Q_c values when the R^2 fit was higher than 0.7.

Each measurement is thus modelled in space using the multiple scattering kernels at a lapse time of 19 s with the Matlab©-based codes proposed by Del Pezzo et al. (2018). The kernels provide the rows of the inversion matrix; each element represents the contribution of a node to the Qc measurement. Before forming the matrix, each kernel is normalized for the total sensitivity, assuming no break of equipartition due to leakage of the energy outside the grid (Margerin, 2017). The model parameters are the Q_C^{-1} at each node of the grids defined in the previous section. The final inversion problems solve a total of 3200 (0.5 km) and 400 (1 km) model parameters. At each frequency we obtain them using a first-order Tikhonov regularised inversion (Fig. 4).

3.3. Resolution and stability testing

Sensitivity analyses and synthetic reconstruction tests are employed to assess the spatial resolution and reliability as well as the robustness of the solution of inverse problems (Rawlinson and Spakman, 2016). The resolution and stability of the inversion solutions were examined by changing the damping parameters and outputting the corresponding images (Figs. S1–S4) and inverting for different node spacings (1 and 0.5 km). The inversion at 0.5 km spacing was under-determined in most of the model, leading to negative inverse quality factors and values of covariances for 70% of the model parameters above 0.1, for an average value of 0.02. We concluded that a regular 0.5-km-spaced grid overestimated the effective resolution achievable with the method. We thus only discuss the results and perform resolution tests on a 1-km-spaced grid, which leads to a mixed-determined inversion.

After looking at the residual vs. solution norm graph (Fig. 4), we tested different damping parameters (from 0.08 to 0.38) by outputting the results at 3 Hz (Fig. S1) and 6 Hz (Fig. S2) and the corresponding checkerboard tests (Figs. S3–S4). A damping parameter of *0.16* gives an optimum resolution between depths of 1 km and 3 km in the centre of the model at 3 Hz (Fig. 4) while providing a sufficient amount of features. The best recovery is available at the lowest central frequency while features at 6 Hz result over-damped (compare Figs. S1–S2). Resolution is almost completely lost at higher frequencies, mainly due to the lack of energy recorded towards the end of the envelope, restricting depth penetration.

4. Results and discussion

4.1. Results

The 3D sensitivity kernels and functions (Eqs. (1)–(3)) described in Section 3.1 were implemented in the inversion. The tomographic analysis reveals that the model is best suited to recover anomalies at 3 Hz. The checkerboard tests (Fig. 5) reveal that the 3-Hz-results are stable between 1.5 km and 3 km depths at the centre of the caldera – predominantly in onshore areas and offshore Monte Nuovo (Fig. 5C–D). The Q_C kernels (Fig. 3) are built using seismic albedo and inverse extinction lengths, B_0 and Le^{-1}, of 0.89 and 0.90: these are in the intervals obtained by Del Pezzo et al. (1995) for the caldera.

Fig. 6a shows the 3D coda attenuation models by meshing the nodes using the Matlab© software. For interpretation, we embed this model in Voxler©. The software allows us to interpolate our nodes with a quadratic interpolant, plot the events nucleated during the unrest (January–April 1984, the same period of data collection), include topography and faults (Fig. 6b). High attenuation anomalies were recovered at 2 km and 3 km depths under Solfatara and Mount Nuovo, two areas of fairly intense fracturing and cross-faulting and dominated by 1983 seismic events (Fig. 2). While high-attenuation anomalies are predominantly onshore, they also extend offshore Solfatara and Mount Nuovo at both depths. The anomalies are separated by a low seismic-attenuation volume centred at Pozzuoli, which is approximately orthogonal to the La Starza fault (Fig. 6b). The seismicity of 1984 (reported on all panels of Figs. 6–7) is associated with this low-attenuation anomaly.

Fig. 5. Checkerboard test with input (left) and output (right) showing as horizontal panels for 0 km, 1 km, 2 km and 3 km in A, B, C and D, respectively. The test inverts for 2×2 km^2 anomalies with a parametrization of 1×1 km^2 cells (left, input; right, output). The thick black line is drawn considering the values and shapes of the Q_C^{-1} anomalies in the output for different damping parameters (Fig. 4). The area contoured by the black line is discussed in the main text. M, P and S are locations of Mount Nuovo, Pozzuoli and Solfatara, respectively. Grey curves represent the coastline.

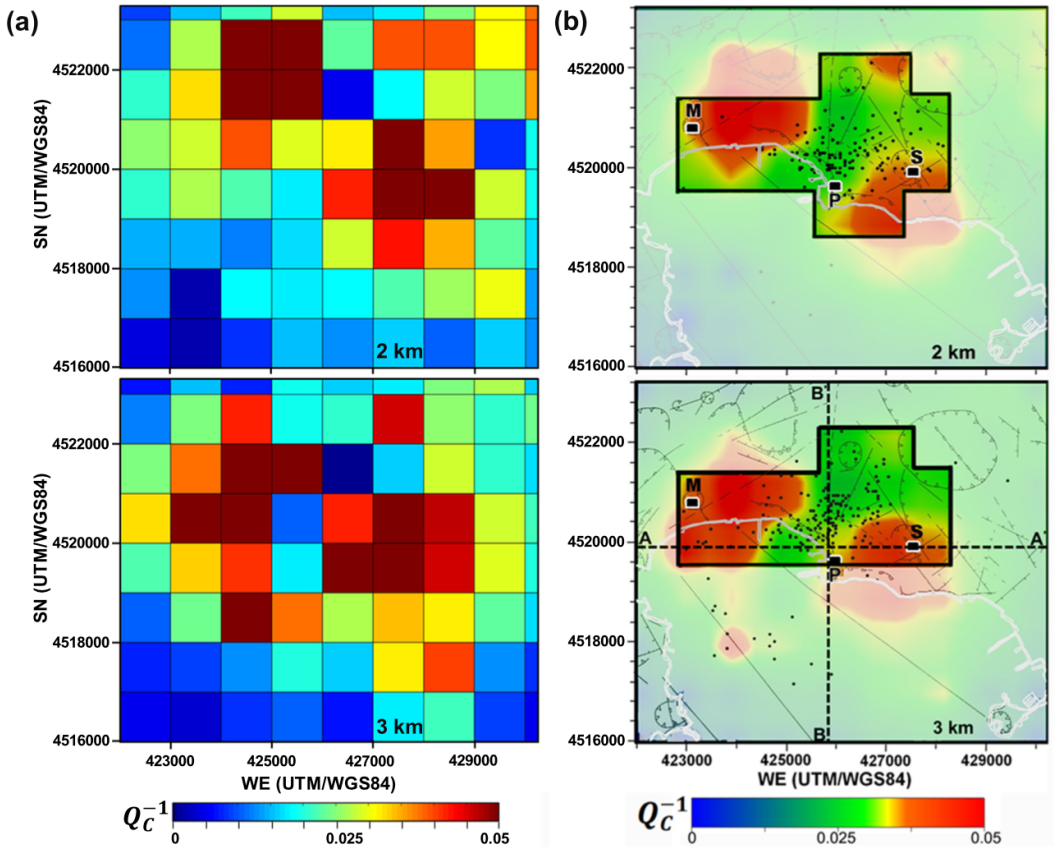

Fig. 6. 3D coda attenuation maps generated for the 1983–1984 seismic unrests at Campi Flegrei caldera. (a) The model is shown as blocks in Matlab© with no interpolation. (b) The model is shown after inserting it in the Voxler© interpretational software. Black solid circles represent the 1984 seismic events superimposed on the tomograms. M, P and S are locations of Mount Nuovo, Pozzuoli and Solfatara, respectively. Thin black lines and curves represent the fracture systems at the caldera. Grey curves represent the coastline. The thick black line highlights the zone resolved by the analysis. Dashed lines A-A′ (W-E) and B-B′ (S—N) are lines of sections shown in Fig. 7.

Vertical W-E (A-A′) and S—N (B-B′) slices (cross-sections – Fig. 7a, b, see Fig. S6) through the caldera reveal more information about the geometry of the attenuation anomalies. The checkerboard tests for the sections (Fig. S5) show locally-improved resolution around 1 km depth, in addition to those observed at 2 km and 3 km depths. Section A-A′ (Fig. 7a) shows that two high-attenuation anomalies are separated by a low-attenuation body between depths of 2 and 3 km. The first is divided into a deep plume-like structure located south of Solfatara up to ~1.8 km (**1**) and a smaller spherical one just west of it (**2**) by a lower-attenuation layer (**3**). The low-attenuation seismic volume (**4**) separates the Solfatara anomaly from that at Monte Nuovo, which stops at ~2 km (**5**). The B-B′ vertical section (Fig. 7b) was chosen to compare our model to Fig. 4a of Calò and Tramelli (2018). It shows that the high-attenuation plume-like body develops offshore, just south of Pozzuoli (Fig. 7b, **1**), producing most of the seismic activity recorded in 1984 (**4**). This image is obtained at 3 Hz, where direct-wave seismic attenuation and single-scattering imaging are affected by biases induced by the high-scattering caldera rim structures (Tramelli et al., 2006; De Siena et al., 2013). Fig. 8 summarizes the observations and interpretations of this study; here, coda-attenuation anomalies are integrated with results of seismic reflections survey (Zollo et al., 2008), seismic tomography, and rock-physics (e.g., Vanorio and Kanitpanyacharoen, 2015; De Siena et al., 2017a, 2017b; Calò and Tramelli, 2018).

4.2. Discussion

The coda attenuation maps can be jointly interpreted with the recent body-wave velocity and attenuation, and single-scattering tomography maps of Calò and Tramelli (2018). In this work, a high Vp/Vs anomaly, separated into a shallow and a deep portions by a low-Vp/Vs interface, is reconstructed below Pozzuoli between depths of 0 and 3.5 km. Calò and Tramelli (2018) efficiently reconstructs (0.5 km resolution) the previously-inferred caprock (Vanorio and Kanitpanyacharoen, 2015) extending across the caldera and blocking deep magmatic fluids rising to the surface (De Siena et al., 2017b). Our coda-attenuation anomalies correlate in space with the Vp/Vs results of Calò and Tramelli (2018). The deeper high-attenuation anomaly south of Solfatara (Fig. 7a, **1**) corresponds to high Vp/Vs ratios and high direct-wave attenuation, which are generally signatures of regions saturated with water or enriched in molten rocks. As the region lies above the deeper (3–4 km) primary seismic and deformation sources (Amoruso et al., 2014; De Siena et al., 2017a, 2017b), its characteristics are likely due to the accumulation of magmatic fluids above a sill (Fig. 8). We thus infer that the high attenuation anomalies below Solfatara (Fig. 7a, **1**) and Monte Nuovo (Fig. 7a, **5**) mark the deep feeders of the respective fumarole fields, likely filled by magmatic gases emanating from depth (Battaglia et al., 2008; De Siena et al., 2010, 2017b). The shallower high-attenuation anomaly (Fig. 7, **2**) is at the limit of our resolution: its features are more extended once we remove interpolation (Fig. S6a, b). Still, the volume is located where hydrothermal reservoirs (Fig. 8) were reconstructed by previous seismic tomography studies (Vanorio et al., 2005; Calò and Tramelli, 2018). These reservoirs have been fed and perturbed by the rising magmatic gases (De Natale et al., 2001) and feed fumarolic vents at Solfatara (Caliro et al., 2007).

The low seismic attenuation layer (Fig. 7, **3**) correlates in space with the caprock (Vanorio and Kanitpanyacharoen, 2015; De Siena et al.,

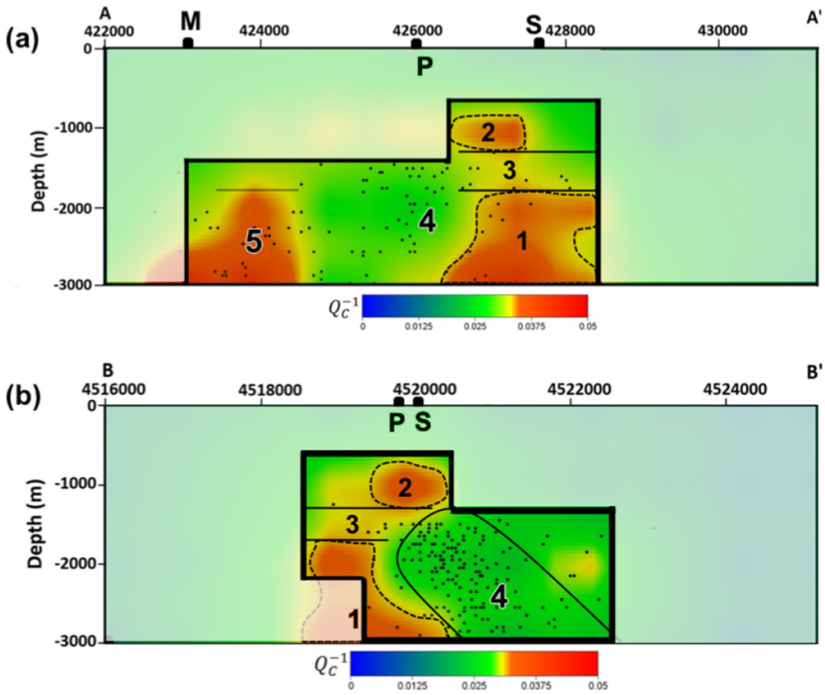

Fig. 7. Cross-sections through lines A-A′ (W-E) and B-B′ (S—N) as shown in Fig. 6. Descriptions are the same as in Fig. 6. The number corresponds to areas discussed in the body of the article. The horizontal lines above and below volume **3** are derived from the high-velocity caprock defined by Calò and Tramelli (2018).

2017b; Calò and Tramelli, 2018) that is currently deforming and allowing the system to release stress above the deformation anomaly (Fig. 8). Calò and Tramelli (2018) reconstruct it below Pozzuoli and Solfatara, with its width thinning under Pozzuoli. We infer that the flattening and horizontal elongation of the deeper high attenuation anomalies below 2 km (**1** and **5**, see also Fig. S6a) is a manifestation of the blocking and spreading around of the rising hot magmatic fluid below the caprock under Monte Nuovo and Solfatara. Monte Nuovo

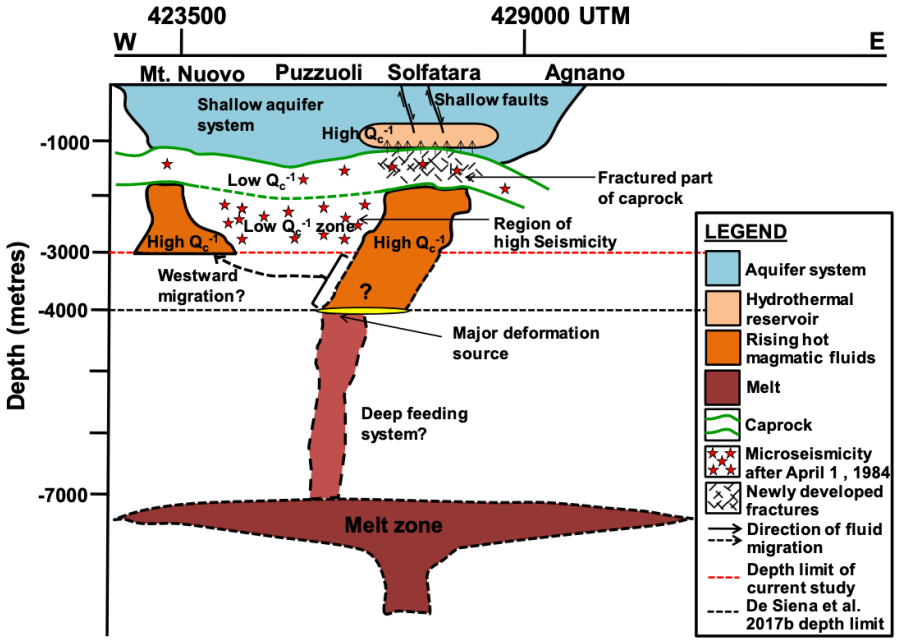

Fig. 8. A West-East sketch of the uppermost crust of Campi Flegrei caldera during the 1983–84 unrest (modified after De Siena et al., 2010). This pictorial summary represents the interpretation based on the results of the current study on coda-attenuation tomography once compared with those from velocity and direct wave attenuation tomography and many other related works on the geological structure of Campi Flegrei. The melt zone shown at −7500 m and the major deformation source at −4000 m were deduced by Zollo et al. (2008), and Amoruso et al. (2014) and De Siena et al. (2017b), respectively. The dashed arrow shows migration of hot fluids below the caprock to perturb the shallow hydrothermal reservoir below Mt. Nuovo (De Siena et al., 2017b). The vertical arrow shows migration of hot fluids across the breached caprock to perturb the shallow hydrothermal reservoir below Solfatara.

lacks the extended network of fractures necessary for fluid to permeate the upper system, possibly due to the remnant of past eruptions.

The SW-to-NE trending low-attenuation anomaly (**4**) corresponds to the part of the high-velocity caprock that dips consistently under Pozzuoli (Calò and Tramelli, 2018). We infer that the high seismicity in the region is a consequence of the stress sustained by the caprock from the 4-km deep deformation source (Fig. 8). Where pre-existing microfractures and faults exist, i.e., in the eastern onshore part of the caldera (Fig. 2), they created pathways for magmatic fluids (Fig. 7) to connect with the shallower reservoir (**2**). Magmatic fluids are thus more likely stored in the subsiding western portion, where they cannot reach the surface, contributing to the high-gravity anomalies of Capuano et al. (2013) at depths of 1.8–2.2 km.

The SW-to-NE trend of the region of low attenuation separating Solfatara from Monte Nuovo (**4**) coincides with that of a high group-velocity anomaly obtained by De Siena et al. (2018). These authors image the 2011–2013 unrest using ambient noise recordings. The location of this high-velocity boundary (at ~ 1 km depth) between eastern and western caldera is shifted east with respect to our high Q_c anomaly in 1983–1984. This shift corresponds to that in seismicity and vent opening, which happened in the last 40 years.

5. Conclusions

This study employs 3D multiple-scattering coda-attenuation kernels to map caldera structures during unrest at Campi Flegrei caldera for the first time. The results unveil the differences in the feeding systems of Solfatara, where hot fluids find pathway to reach the surface from a deeper high-deformation source, and Monte Nuovo, where they are stored by a thicker, possibly less fractured caprock. The low-attenuation caprock presents a heterogeneous structure, with a low attenuation body dipping under Pozzuoli town. Most of the seismicity during the unrest nucleated in this region. As the main source of deformation is located SE of Pozzuoli (Amoruso et al., 2014), we infer that this low-attenuation body blocked most of the materials rising westward and northward from depth. The work confirms that the caprock acts as the principal blocking interface throughout the caldera, with a shallow high-attenuation reservoir active as a feeder for fumaroles at Solfatara.

The study allows us to model coda envelope at a lower frequency (3 Hz) than done before, going over a diffusive, homogeneous approximation. Due to the higher sensitivity of seismic attenuation to heterogeneous structures, this application offers a new tool to image extended geothermal reservoirs, especially the structures confining them. The development of a fluid-flow model based on these findings may provide better data for estimating the reservoir potential and the hazards that the stored fluids bring.

Acknowledgements

W. G. Akande acknowledges the financial support of his sponsor, the Petroleum Technology Development Fund (PTDF), for his research. L. De Siena received the Public Engagement for Early Career Researchers funding from the Scottish Alliance for Geosciences Environment (SAGES) to collect data and discuss the results of the present work. We thank Edoardo Del Pezzo and Angel De La Torre for providing the codes necessary to compute the three-dimensional kernels using Paasschens' equations. The support of the editor, Diana Roman, and constructive remarks of two anonymous reviewer helped us constrain our interpretation, highlight the novelty of our approach, and avoid resolution biases.

Appendix A. Supplementary data

Supplementary data to this article can be found online at https://doi.org/10.1016/j.jvolgeores.2019.06.007.

References

AGIP, 1987. Modello geotermico del sistema flegreo. Servizi Centrali per l'Esplorazione, SERG-MESG. Agip Oil Company, San Donato (23 pp. (in Italian)).
Aiello, G., Marsella, E., Di Fiore, V., Cicchella, A.G., 2014. The regional geological structure of the Campania continental margin inferred by deep multichannel seismic profiles. GNGTS, Sessione 3 (1), 22–27.
Aki, K., Chouet, B., 1975. Origin of coda waves: source, attenuation, and scattering effects. J. Geophys. Res. 80 (23), 3322–3342.
Amoruso, A., Crescentini, L., Berrino, G., 2008. Simultaneous inversion of deformation and gravity changes in a horizontally layered half-space: evidences for magma intrusion during the 1982–1984 unrest at Campi Flegrei caldera (Italy). Earth Planet. Sci. Lett. 272 (1–2), 181–188. https://doi.org/10.1016/j.epsl.2008.04.040.
Amoruso, A., Crescentini, L., Sabbetta, I., De Martino, P., Obrizzo, F., Tammaro, U., 2014. Clues to the cause of the 2011–2013 Campi Flegrei caldera unrest, Italy, from continuous GPS data. Geophys. Res. Lett. 41, 3081–3088. https://doi.org/10.1002/2014GL059539.
Aster, R., Meyer, R., Natale, G.D., Martini, M., Del Pezzo, E., Iannaccone, G., Scarpa, R., 1989. Seismic investigation of the Campi Flegrei: a synthesis and summary of results. In: Aki, K., Gasparini, P., Scarpa, R. (Eds.), Volcanic Seismology. Proc. Volc. Series III. Springer-Verlag, Switzerland AG, pp. 462–483.
Barberi, F., Innocenti, F., Lirer, L., Munno, R., Pescatore, T., Santacroce, R., 1978. The Campanian Ignimbrite: a major prehistoric eruption in the Neapolitain area (Italy). Bull. Volcanol. 41 (1), 1–22.
Battaglia, J., Zollo, A., Virieux, J., Iacono, D.D., 2008. Merging active and passive data sets in travel-time tomography: the case study of Campi Flegrei caldera (Southern Italy). Geophys. Prospect. 56, 555–573. https://doi.org/10.1111/j.1365-2478.2007.00687.x.
Bianco, F., Del Pezzo, E., Castellano, M., Ibanez, J., Di Luccio, F., 2002. Separation of intrinsic and scattering seismic attenuation in the Southern Apennine zone, Italy. Geophys. J. Int. 150, 10–22.
Borleanu, F., De Siena, L., Thomas, C., Popa, M., Radulian, M., 2017. Seismic scattering and absorption mapping from intermediate-depth earthquakes reveals complex tectonic interactions acting in the Vrancea region and surroundings (Romania). Tectonophysics 706-707, 129–142.
Brocchini, D., Principe, C., Castradori, D., Laurenzi, M.A., Gorla, L., 2001. Quaternary evolution of the southern sector of the Campanian Plain and early Somma-Vesuvius activity, insights from the Trecase-1 well. Miner Petrol 73, 67–91.
Caliro, S., Chiodini, G., Moretti, R., Avino, R., Granieri, D., Russo, M., Fiebig, J., 2007. The origin of the fumaroles of La Solfatara (Campi Flegrei, South Italy). Geochim. Cosmochim. Acta 71 (12), 3040–3055. https://doi.org/10.1016/j.gca.2007.04.007.
Calò, M., Tramelli, A., 2018. Anatomy of the Campi Flegrei caldera using Enhanced Seismic Tomography Models. Sci. Rep. 8 (16254), 1–12. https://doi.org/10.1038/s41598-018-34456-x.
Calvet, M., Margerin, L., 2013. Lapse-time dependence of coda Q: anisotropic multiple-scattering models and application to Pyrenees. Bull. Seismol. Soc. Am. 103 (3), 1993–2010. https://doi.org/10.1785/0120120239.
Calvet, M., Sylvander, M., Margerin, L., Villasenor, A., 2013. Spatial variations of seismic attenuation and heterogeneity in the Pyrenees: Coda Q and peak delay time analysis. Tectonophysics 608, 428–439. https://doi.org/10.1016/j.tecto.2013.08.045.
Capuano, P., Russo, G., Civetta, L., Orsi, G., D'Antonio, M., Moretti, R., 2013. The active portion of the Campi Flegrei caldera structure imaged by 3-D inversion of gravity data. Geochemistry, Geophysics & Geosystems 14 (10), 4681–4697. https://doi.org/10.1002/ggge.20276.
Carlino, S., Piochi, M., Tramelli, A., Mormone, A., Montanaro, C., Scheu, B., Klaus, M., 2018. Field-scale permeability and temperature of volcanic crust from borehole data: Campi Flegrei, southern Italy. J. Volcanol. Geotherm. Res. 357, 276–286.
De Lorenzo, S., Gasparini, P., Mongelli, F., Zollo, A., 2001. Thermal state of the Campi Flegrei caldera inferred from seismic attenuation tomography. J. Geodyn. 32 (4–5), 467–486.
De Natale, G., Troise, C., Pingue, F., 2001. A mechanical fluid-dynamic model for ground movements at Campi Flegrei caldera. J. Geod. 32, 487–517.
De Siena, L., Del Pezzo, E., Bianco, F., Tramelli, A., 2009. Multiple resolution seismic attenuation imaging at Mt. Vesuvius. Phys. Earth Planet. Inter. 173, 17–32.
De Siena, L., Del Pezzo, E., Bianco, F., 2010. Campi Flegrei seismic attenuation image: evidences of gas reservoirs, hydrothermal basins and feeding systems. J. Geophys. Res. 115, 9312–9329.
De Siena, L., Del Pezzo, E., Thomas, C., Curtis, A., Margerin, L., 2013. Seismology Seismic energy envelopes in volcanic media: in need of boundary conditions. Geophys. J. Int. 195, 1102–1119. https://doi.org/10.1093/gji/ggt273.
De Siena, L., Thomas, C., Waite, G.P., Moran, S.C., Klemme, S., 2014a. Attenuation and scattering tomography of the deep plumbing system of Mount St. Helens. J. Geophys. Res. Solid Earth 119, 8223–8238. https://doi.org/10.1002/2014JB011372.
De Siena, L., Thomas, C., Aster, R., 2014b. Multi-scale reasonable attenuation tomography analysis (MuRAT): an imaging algorithm designed for volcanic regions. J. Volcanol. Geotherm. Res. 277, 22–35.
De Siena, L., Amoruso, A., Pezzo, E.D., Wakeford, Z., Castellano, M., Crescentini, L., 2017a. Space-weighted seismic attenuation mapping of the aseismic source of Campi Flegrei 1983–1984 unrest. Geophys. Res. Lett. 44, 1740–1748. https://doi.org/10.1002/2017GL072507.
De Siena, L., Chiodini, G., Vilardo, G., Del Pezzo, E., Castellano, M., Colombelli, S., Tisato, N., Ventura, G., 2017b. Source and dynamics of a volcanic caldera unrest: Campi Flegrei, 1983–84. Sci. Rep. 7 (8099), 1–13. https://doi.org/10.1038/s41598-017-08192-7.
De Siena, L., Sammarco, C., Cornwell, D.G., La Rocca, M., Bianco, F., Zaccarelli, L., Nakahara, H., 2018. Ambient seismic noise image of the structurally controlled heat and fluid feeder pathway at Campi Flegrei caldera. Geophys. Res. Lett. 45, 6428–6436. https://doi.org/10.1029/2018GL078817.

Del Pezzo, E., Ibanez, J.M., Morales, J., Akinci, A., Maresca, R., 1995. Measurements of intrinsic and scattering seismic attenuation in the crust. Bull. Seismol. Soc. Am. 85 (5), 1373–1380.
Del Pezzo, E., Bianco, F., Zaccarelli, L., 2006. Separation of Qi and Qs from passive data at Mt. Vesuvius: a reappraisal of the seismic attenuation estimates. Phys. Earth Planet. Inter. 159 (3–4), 202–212. https://doi.org/10.1016/j.pepi.2006.07.005.
Del Pezzo, E., Bianco, F., Marzorati, S., Augliera, P., D'Alema, E., Massa, M., 2011. Depth-dependent intrinsic and scattering seismic attenuation in north central Italy. Geophysics Journal International 186, 373–381.
Del Pezzo, E., Ibañez, J., Prudencio, J., Bianco, F., De Siena, L., 2016. Absorption and scattering 2-D volcano images from numerically calculated space-weighting functions. Geophys. J. Int. 206, 742–756.
Del Pezzo, E., De La Torre, A., Bianco, F., Ibanez, J., Gabrielli, S., De Siena, L., 2018. Numerically calculated 3-D space-weighting functions to image crustal volcanic structures using diffuse coda waves. Geosciences 8 (5), 175–187. https://doi.org/10.3390/geosciences8050175.
Margerin, L., 2017. Breakdown of equipartition in diffuse fields caused by energy leakage. The European Physical Journal Special Topics 226 (7), 1353–1370. https://doi.org/10.1140/epjst/e2016-60165-6.
Margerin, L., Planes, P., Mayor, J., Calvet, M., 2015. Seismology Sensitivity kernels for coda-wave interferometry and scattering tomography: theory and numerical evaluation in two-dimensional anisotropically scattering media. Geophys. J. Int. 204, 650–666. https://doi.org/10.1093/gji/ggv470.
Mayor, J., Calvet, M., Margerin, L., Vanderhaeghe, O., Traversa, P., 2016. Crustal structure of the Alps as seen by attenuation tomography. Earth Planet. Sci. Lett. 439, 71–80. https://doi.org/10.1016/j.epsl.2016.01.025.
Mukhopadhyay, S., Sharma, J., Del Pezzo, E., Kumar, N., 2010. Study of attenuation mechanism for Garwhal-Kumaun Himalayas from analysis of coda of local earthquakes. Phys. Earth Planet. Inter. 180, 7–15.
Nishigami, K., 1991. A new inversion method of coda waveforms to determine spatial distribution of coda scatterers in the crust and uppermost mantle. Geophys. Res. Lett. 18, 2225–2228.
Orsi, G., Gallo, G., Zanchi, A., 1991. Simple-shearing block resurgence in caldera depression. A model from Pantelleria and Ischia. J. Volcanol. Geotherm. Res. 47, 1–11. https://doi.org/10.1016/0377-0273(91)90097-J.
Orsi, G., Vita, S.D., Vito, M.D., 1996. The restless resurgent Campi Flegrei caldera (Italy): constraints on its evolution and configuration. J. Volcanol. Geotherm. Res. 74, 179–214.
Paasschens, J., 1997. Solution of the time-dependent Boltzmann equation. Phys. Rev. E 56, 1135–1141. https://doi.org/10.1103/PhysRevE.56.1135.
Padhy, S., Subhadra, N., 2013. Separation of intrinsic and scattering seismic wave attenuation in Northeast India. Geophys. J. Int. 195, 1892–1903. https://doi.org/10.1093/gji/ggt350.
Piochi, M., Kilburn, C.R.J., Di Vito, M.A., Mormone, A., Tramelli, A., Troise, C., De Natale, G., 2014. The volcanic and geothermally active Campi Flegrei caldera: an integrated multidisciplinary image of its buried structure. Int. J. Earth Sci. (Geol Rundsch) 103, 401–421. https://doi.org/10.1007/s00531-013-0972-7.
Prudencio, J., Del Pezzo, E., García-Yeguas, A., Ibáñez, J.M., 2013a. Spatial distribution of intrinsic and scattering seismic attenuation in active volcanic islands –I: model and the case of Tenerife Island. Geophys. J. Int. 195 (3), 1942–1956. https://doi.org/10.1093/gji/ggt361.
Prudencio, J., Ibáñez, J.M., García-Yeguas, A., Del Pezzo, E., Posadas, A.M., 2013b. Spatial distribution of intrinsic and scattering seismic attenuation in active volcanic islands – II: deception Island images. Geophys. J. Int. 195 (3), 1957–1969. https://doi.org/10.1093/gji/ggt360.
Prudencio, J., Del Pezzo, E., Ibáñez, J.M., Giampiccolo, E., Patané, D., 2015a. Two-dimensional seismic attenuation images of Stromboli Island using active data. Geophys. Res. Lett. 42, 1717–1724. https://doi.org/10.1002/2015GL063293.
Prudencio, J., De Siena, L., Ibanez, J.M., Del Pezzo, E., 2015b. The 3D attenuation structure of Deception Island (Antarctica). Surv. Geophys. 36, 371–390. https://doi.org/10.1007/s10712-015-9322-6.
Prudencio, J., Ibáñez, J.M., Del Pezzo, E., Martí, E.J., García-Yeguas, A., De Siena, L., 2015c. 3D attenuation tomography of the volcanic island of Tenerife (Canary Islands). Surv. Geophys. 36 (5), 693–716. https://doi.org/10.1007/s10712-015-9333-3.
Prudencio, J., Aoki, Y., Takeo, M., Ibáñez, J.M., Del Pezzo, E., Song, W., 2017a. Separation of scattering and intrinsic attenuation at Asama volcano (Japan): evidence of high volcanic structural contrasts. J. Volcanol. Geotherm. Res. 333, 96–103.
Prudencio, J., Taira, T., Aoki, Y., Aoyama, H., Onizawa, S., 2017b. Intrinsic and scattering attenuation images of Usu volcano. Japan. Bulletin of Volcanology 79 (29), 1–12. https://doi.org/10.1007/s00445-017-1117-9.
Prudencio, J., Manga, M., Taira, T., 2018. Subsurface structure of Long Valley caldera imaged with seismic scattering and intrinsic attenuation. Journal of Geophysical Research: Solid Earth 123, 5987–5999. https://doi.org/10.1029/2017JB014986.
Rawlinson, N., Spakman, W., 2016. On the use of sensitivity tests in seismic tomography. Geophys. J. Int. 205 (2), 1221–1243. https://doi.org/10.1093/gji/ggw084.
Sato, H., Fehler, M.C., Maeda, T., 2012. Seismic Wave Propagation and Scattering in the Heterogeneous Earth. Second edition. Springer-Verlag, Berlin Heidelberg (511pp).
Spencer, J.J.W., 1981. Stress relaxation at low frequencies in fluid-saturated rocks: attenuation and modulus dispersion. J. Geophys. Res. 86, 1803–1812. https://doi.org/10.1029/JB086iB03p01803.
Tramelli, A., Del Pezzo, E., Bianco, F., Boschi, E., 2006. 3D scattering image of the Campi Flegrei caldera (Southern Italy): new hints on the position of the old caldera rim. Phys. Earth Planet. Inter. 155 (3–4), 269–280. https://doi.org/10.1016/j.pepi.2005.12.009.
Vanorio, T., Kanitpanyacharoen, W., 2015. Rock physics of fibrous rocks akin to Roman concrete explains uplifts at Campi Flegrei Caldera. Science 349 (6248), 617–621. https://doi.org/10.1126/science.aab1292.
Vanorio, T., Virieux, J., Capuano, P., Russo, G., 2005. Three-dimensional seismic tomography from P-wave and S-wave microearthquake travel times and rock physics characterization of the Campi Flegrei Caldera. J. Geophys. Res. 110 (B03201), 1–14. https://doi.org/10.1029/2004JB00310.
Vargas, C.A., Mann, P., 2013. Tearing and breaking off of subducted slabs as the result of collision of the Panama Arc-Indenter with Northwestern South America. Bull. Seismol. Soc. Am. 513 (103(3)), 2025–2046. https://doi.org/10.1785/0120120328.
Vargas, C.A., Pujades, L., Caneva, A., 2012. Attenuation structure of the Galeras Volcano, Colombia. Boletín de Geología 34 (2), 149–161.
Winkler, K., Nur, A., 1979. Pore fluids and seismic attenuation in rocks. Geophys. Res. Lett. 6 (1), 1–4.
Zollo, A., Maercklin, N., Vassallo, M., Dello Iacono, D., Virieux, J., Gasparini, P., 2008. Seismic reflections reveal a massive melt layer feeding Campi Flegrei caldera. Geophys. Res. Lett. 35 (L12306), 1–6. https://doi.org/10.1029/2008GL034242.